Laser-induced trapping of chlorine molecules with pico- and femtosecond pulses

M. Schmidt, D. Normand, and C. Cornaggia
Commissariat à l'Energie Atomique, DSM/DRECAM/SPAM, Bâtiment 522, Centre d'Etudes Nucléaires de Saclay, 91191 Gif-sur-Yvette CEDEX, France
(Received 8 July 1994)

We have studied the multielectron dissociative ionization of Cl_2 with intense 130-fs laser pulses at 395, 610, and 790 nm, and 2-ps pulses at 610 nm. The kinetic-energy releases and the fragmentation branching ratios are found to be essentially independent of the laser wavelength and of the pulse duration. Moreover, for all fragmentation channels up to $Cl_2^{8+} \rightarrow Cl^{4+} + Cl^{4+}$, the measured energy releases are systematically 70% of those expected from a simple Coulomb explosion of the molecule at its neutral ground-state equilibrium internuclear distance. This constant-energy ratio is even more surprising in the picosecond regime, where the pulse duration largely exceeds the molecular ground-state vibrational period by a factor of 30 so that the molecular motions cannot be considered as frozen during interaction. The results are tentatively explained in terms of laser-induced stabilization of the transient molecular species via charge-resonance or charge-transfer couplings. In this picture, the electron removal occurs at the end of the laser pulse, leading only then to the explosion of the multicharged ions.

PACS number(s): 33.80.Rv, 33.80.Wz, 42.50.Hz

I. INTRODUCTION

When submitted to an intense (sub-) picosecond laser field, molecules in the gas phase become multiply ionized and explode into fragments. This process is commonly called multielectron dissociative ionization (MEDI). The molecular ions, which are formed during the MEDI interaction, are transient species with lifetimes too short to be detected. The use of correlation techniques, however, allows us to trace back the fragmentation dynamics to an early stage, by identification of all the different ionic fragments proceeding from the same transient species. During the fragmentation, the potential energy of the transient ion is converted into the kinetic energy of the fragments. Once the fragmentation channels are identified, the kinetic-energy releases can be deduced from the measurement of the fragment velocities.

The high complexity of MEDI interactions renders a theoretical description extremely difficult. The simplest way to describe the molecular response is to use the point-charge model. In this model the electron removal is supposed to occur at the neutral-molecule internuclear separation R_e, and the nuclear point charges of the transient molecular ions are only submitted to electrostatic forces. In the case of diatomic molecules, the kinetic energy released from the $AB^{(p+q)+}$ transient ion dissociating into the fragments A^{p+} and B^{q+} is then simply given by $E_{\mathrm{Cb}}[\mathrm{eV}] = 14.4pq/R_e[\mathrm{\AA}]$, where E_{Cb} is commonly referred to as *Coulomb energy* and p,q are the unit charges of the two atomic fragments.

All the MEDI experiments, however, have systematically shown that the measured kinetic-energy releases E_{expt} are significantly lower than those (E_{Cb}) predicted by the point-charge model. In most cases [1,2], the energy ratio $E_{\mathrm{expt}}/E_{\mathrm{Cb}}$ is in the range of 40% to 50%, and only in the case of iodine is the mismatch between E_{expt} and E_{Cb} less important [3].

In the adopted picture so far, the MEDI interaction is governed by the competition between the electron removal and the dissociation of the molecular transient ions. In order to account for the observed kinetic-energy defect, the molecular ions AB^{n+} are assumed to be formed on Coulombic states at increasing internuclear distances for increasing charge n [4,5]. Moreover, if the laser field is still present after dissociation, the fragments are further ionized before they leave the interaction zone. Provided that this so-called post-dissociation ionization (PDI) of the fragments is total, the energy defect is also due to an experimental artifact, which leads to a comparison of the energy release measured for the $(p,q-1)$ channel:

$$\begin{aligned} &AB^{(p+q-1)+} \rightarrow A^{p+} + B^{(q-1)+} + E_{\mathrm{expt}}(p,q-1) \\ &B^{(q-1)+} \rightarrow B^{q+} , \end{aligned} \tag{1}$$

with the Coulomb value expected for the (p,q) channel:

$$AB^{(p+q)+} \rightarrow A^{p+} + B^{q+} + E_{\mathrm{expt}}(p,q) . \tag{2}$$

The two processes obviously yield the same fragments A^{p+} and B^{q+}, but different kinetic-energy releases.

In the above classic picture, Coulomb energies can only be reached in the interaction of extremely short pulses with heavy molecules, which leads to freezing of the internuclear distance and to suppression of PDI, since dissociation occurs in field-free conditions [6]. However, the classic picture fails to account for two experimental observations: (i) the independence of kinetic-energy releases versus the laser pulse duration [7], and (ii) the nature of the chemical bonds that influences the characteristics of the MEDI processes [8] even in the long-pulse regime, indicating that the molecular ions are formed at, or close to, the equilibrium internuclear separation R_e.

In the present paper we propose an alternative picture of the MEDI dynamics that is consistent with all experimental findings. This picture is supported by our experimental data on the chlorine molecule performed with femto- and picosecond laser pulses. The time scale of interaction is then respectively comparable or much longer than the neutral ground-state vibrational period (60 fs) of the molecule.

II. EXPERIMENT

The experiment is performed with femtosecond laser pulses ($\Delta\tau \leq 130$ fs) at 395, 610, and 790 nm, and with picosecond pulses ($\Delta\tau = 2$ ps) at 610 nm. The femtosecond laser source is based on a commercial Ti:sapphire (Ti:Sa) system (Continuum) of the DRECAM laser facility delivering pulses of 130-fs duration at 790 nm with an energy E of 2 mJ at a repetition rate of 20 Hz. The 395-nm pulses are obtained by frequency-doubling of the Ti:Sa fundamental radiation with a 0.5-mm-thick BBO crystal. Typically, we obtained pulses of 130-fs duration with $E = 400$ μJ. The 610-nm pulses ($\Delta\tau = 100$ fs, $E = 350$ μJ) are generated from a white-light continuum amplified in three neodymium-doped yttrium aluminum garnet pumped dye cells. The picosecond synchropumped dye laser system, delivering 2-ps pulses ($E = 2.5$ mJ) at 610 nm at a rate of 10 Hz, has already been described in detail [5]. The picosecond laser beam is focused with an $f = 50$ mm parabolospheric lens yielding a maximum peak intensity of 5×10^{15} W/cm^2, whereas the femtosecond lasers are focused with an $f = 60$ mm achromatic lens to avoid lengthening of the femtosecond pulses [9] (peak intensity $\leq 2\times10^{16}$ W/cm^2 at 790 nm and $\approx 5\times10^{15}$ W/cm^2 at both 395 and 610 nm).

The time-of-flight (TOF) mass-spectrometer [5], with a double acceleration chamber and a 20-cm-long drift tube, offers both good energy resolution and high collection efficiency. The acceleration fields in the two chambers (100 and 400 V/cm) are determined by computer simulations to ensure linear dependence of the ion TOF's on the ion initial axial velocities. The ion current is detected with an electron multiplier (Philips XP 1600) through an adjustable aperture and is digitalized by a numerical oscilloscope (Lecroy 9350) with a sampling rate of 1 GHz. All spectra presented are obtained as an average over 1000 laser shots.

The ion energy measurement is based on the forward-backward splitting of the laser-aligned ionic fragments when the laser polarization is set parallel to the spectrometer axis [10,11]. The accuracy of the energy measurements is significantly improved by reducing the aperture in front of the detector down to 3 mm in order to discriminate off-axis ions. To keep away from space-charge effects, the ion spectra are always recorded at various pressures to make sure that the ion splittings are independent of the gas density. The absolute error of our energy measurements is estimated to be better than 5% for the main peaks, and better than 10% for the weakest peaks. The assignments of the fragmentation channels are confirmed using the covariance mapping technique [12]. For these measurements, demanding high ion collection efficiency, the detector aperture is set widely open ($\varnothing = 10$ mm). For practical reasons, i.e., reducing the number of data points to limit the computer calculation time, the sampling rate is reduced to 100 MHz (Lecroy 9400) in these experiments.

III. EXPERIMENTAL RESULTS

Figure 1 shows a typical TOF mass-spectrum obtained from the interaction of Cl_2 with 130-fs Ti:Sa laser pulses at 790 nm and for a laser intensity of 2×10^{16} W/cm^2. The laser polarization vector is set parallel (a) or perpendicular (b) to the ion detection axis. The spectrum is dominated by the three Cl_2^+ molecular-ion peaks, shown in the inset, corresponding to the different isotopic combinations $^{35}Cl_2$, $^{35}Cl^{37}Cl$, and $^{37}Cl_2$ ($m = 70$, 72, and 74, respectively) with the expected abundance ratio 9:6:1. Each $^{35}Cl^{q+}$ peak is accompanied by a three times smaller isotope peak $^{37}Cl^{q+}$ [Fig. 1(a)]. Obviously, the chosen electric field (100 V/cm) in the interaction zone avoids an overlap of the isotopic peaks for $q \geq 2$, since the forward $^{37}Cl^{q+}$ peak appears in between the forward and backward $^{35}Cl^{q+}$ peaks, whereas the backward $^{37}Cl^{q+}$ peak comes last. The most prominent ion peaks around the expected Cl^+-peak positions in the mass-spectrum (TOF ≈ 5.7 μs) obtained for $\parallel$ polarization [Fig. 1(a)] clearly persist for $\perp$ polarization [Fig. 1(b)]. This behavior is characteristic of ion peaks with zero kinetic energy. Indeed, the four peaks correspond to the three Cl_2^{2+} ion peaks with $m/q = 35$, 36, 37 and two weak superimposed HCl^+ peaks at $m/q = 36$ and 38.

The existence of metastable states of Cl_2^{2+} is not surprising, since electron bombardment experiments have previously shown lifetimes of several tens of μs [13]. These states have been assigned to the $1\,^1\Delta_g$ and $1\,^1\Sigma_g^+$ singlet states of Cl_2^{2+}, lying 33 eV above the Cl_2 ground state [14]. The population of these states is highly favored by Franck-Condon transitions since they have about the same equilibrium internuclear distance as the $X\,^1\Sigma_g^+$ neutral ground state. Nevertheless, the $1\,^1\Delta_g$ and $1\,^1\Sigma_g^+$ states become repulsive at large internuclear separations and dissociate into $Cl^+(^3P_g) + Cl^+(^3P_g)$.

The existence of the two chlorine isotopes permits us to distinguish between Cl^+ ions with zero kinetic energy and Cl_2^{2+} ions due to the presence of the $m/q = 36$ ion peak. Note that this is generally impossible in the case of homonuclear molecules. The only Cl^+ peaks observable in Fig. 1(a) are the two forward $^{35}Cl^+$ peaks and the corresponding backward peaks of $^{37}Cl^+$.

A. Kinetic-energy releases in the femtosecond regime

A detailed analysis of the Cl^+ ions is performed by subtracting the mass spectrum recorded in $\perp$ polarization from that obtained in $\parallel$ polarization to suppress ions with zero kinetic energy. The resulting difference spectrum [Fig. 2(a)] is still quite complicated, but a careful analysis reveals that four different Cl^+ energies, i.e., 16 Cl^+ peaks, must be involved (with some residual contributions of the four molecular-ion peaks). Figure 2(b) shows all these peaks which contribute to the simulated spec-

trum. Note that the simulated spectrum, obtained as the superposition of all these ion peaks, underlies the following constraints: (1) forward-backward peak symmetry, (2) full width of 30 ns at half maximum for all peaks, and (3) respect of the $^{35}Cl^+$:$^{37}Cl^+$ abundance ratio. In Fig. 2(a), the resulting sum spectrum is compared to the experimental spectrum. From this analysis, we can assign two low-energetic Cl^+ decay paths involving neutral atoms (0.3 and 0.8 eV, respectively), and two classes of Cl^+ fragments from Coulomb explosion with an energy of 2.5 and 5.3 eV, respectively.

The energetic analysis of the multiply charged fragments [Figs. 3(a)–3(c)] is much more straightforward, since all ion signals are suppressed in ⊥ polarization [Fig. 1(b)], proving that they all correspond to fast atomic fragments. For the sake of clarity, all the $^{37}Cl^{q+}$ peaks are plotted in dashed lines, whereas the prevailing $^{35}Cl^{q+}$ peaks appear in solid lines. The ion peaks are rather sharp, which makes the energy measurements quite accurate, and the ion series due to the ^{37}Cl isotope provides a control measurement of the ion energies. Generally, each Cl^{q+} ($q \geq 2$) peak is composed of three subpeaks that can be easily assigned. For a given Cl^{q+} the subpeak of lowest energy corresponds to the $(q-1,q)$ fragmentation channel, the middle subpeak to the (q,q) channel, and the subpeak of highest energy to the $(q,q+1)$ channel. Interestingly, in addition to these main decay paths of chlorine, which are all charge-symmetric (i.e., the two fragment charges differ by one charge at most), a very weak asymmetric channel (2,4) is also observed. Indeed, Fig. 4, which shows an enlarged view of the Cl^{2+} [Fig. 4(a)] and Cl^{4+} [Fig. 4(b)] spectra on the same energy scale, strongly suggests a correlation of these two ion fragments, both having an energy of 20.5 eV. Moreover, the $^{35}Cl^{2+}$ and $^{35}Cl^{4+}$ peak surfaces at 20.5 eV are equal (after correction for the ion-detector response), which further confirms the existence of the (2,4) channel. Nevertheless, on the basis of the ion-peak surface measurements, it must be stressed that the (2,4) channel is about 15 times weaker than the symmetric (3,3) decay channel of Cl_2^{6+} (for $I=2\times10^{16}$ W/cm^2).

Table I shows the identified fragmentation channels for molecular ions up to Cl_2^{8+} and the measured respective kinetic-energy releases E_{expt} obtained at 790 nm. The assignment of these main chlorine fragmentation pathways is confirmed using the covariance mapping technique. Note, however, that covariance mapping does not allow detection of very weak decay paths, since the covariance signals depend on the product of the two correlated ion signals. For example, the covariance signal associated with the (2,4) channel is roughly 200 times weaker than that of the (3,3) channel.

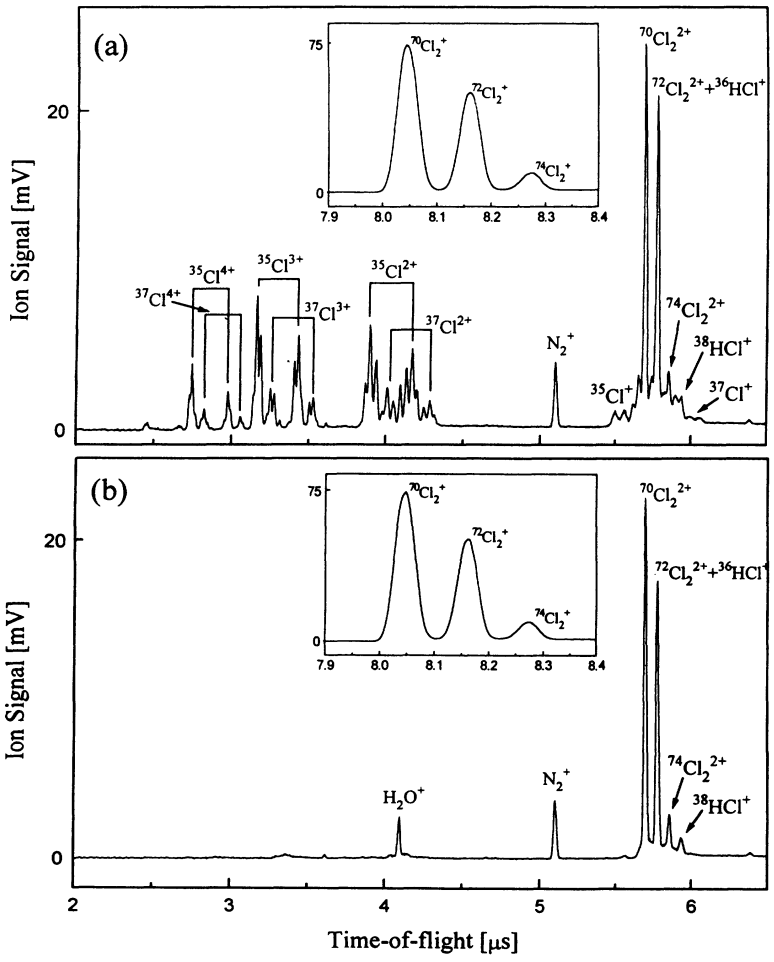

FIG. 1. TOF mass spectra obtained from the MEDI of Cl_2 recorded with 130-fs pulse duration, 790-nm wavelength, and 2×10^{16} W/cm^2 laser intensity. The laser polarization is set (a) parallel or (b) perpendicular to the detection axis. The extraction field in the interaction zone is 100 V/cm and the Cl_2 pressure is 2×10^{-7} Torr. A global peak assignment is given in the figure. The inset shows the three isotopic peaks ($m/q=70,72,74$) of the singly charged molecular chlorine for (a) parallel and (b) perpendicular polarization.

The energy releases E_{expt} of the different decay channels are compared to the Coulomb energies E_{Cb} for the ground-state internuclear distance $R_e = 2.0$ Å (Table I). Most interestingly, a high and almost constant energy ratio E_{expt}/E_{Cb} of 70% is found for all fragmentation channels. The constant energy ratio E_{expt}/E_{Cb} observed in our experiment suggests that the Coulomb repulsion between the ions is the main physical process governing the molecular explosion. However, in order to reproduce the E_{expt} values, one has to assume either that the multiphoton-ionization steps occur along a vertical path at the internuclear distance of $1.4 \times R_e$, or that the Coulomb potential affecting each ion corresponds to an effective charge q_{eff} of the correlated ion, which is given by $0.84 \times q$.

B. Influence of the laser wavelength

The MEDI of Cl_2 has been investigated at three laser wavelengths, namely 395, 610, and 790 nm, with pulse durations of 130, 100, and 130 fs, respectively. Figure 5 shows a comparison of the whole TOF spectra, while Fig. 6 focuses on the more highly charged fragments. In all spectra, the laser polarization vector is set parallel to the ion detection axis, and the laser intensity is of the order of 10^{15} W/cm^2. More precisely, the laser intensity is close to 2×10^{15} W/cm^2 at 790 and 395 nm, but it approaches 5×10^{15} W/cm^2 at 610 nm. There is obviously a strong influence of the laser wavelength on the population of the metastable doubly charged molecular ions. Indeed, at 790 and 610 nm, these metastable ions are widely prominent [Figs. 5(a) and 5(b)]. In the spectrum at 395 nm; however, the low-energy Cl^+ fragments ($E = 0.33$ eV) are largely dominant with characteristic forward-backward peaks around 5.75 μs. These fragments, assigned to a (1,0) decay path involving a neutral partner (Sec. III A) are also present at 790 nm (Fig. 2) but are much weaker. When comparing the spectra in Fig. 6 it is obvious that the slow Cl^+ fragments do not influence the production of the more highly charged ions. Whatever the laser wavelength, we observe the same kinetic energies for the fragments corresponding to the same (p,q) fragmentation channel, and even the branching ratios of the different decay paths are roughly the same. For femtosecond pulses, we can conclude that the kinetic-energy releases represent 70% of the Coulomb energies, without significant effect of the laser wavelength, except for the population of the Cl_2^{2+} metastable ions.

C. Influence of the laser pulse duration

The time scale of our experiment ($\Delta\tau \geq 100$ fs) is too long to essentially freeze the molecular motions of Cl_2

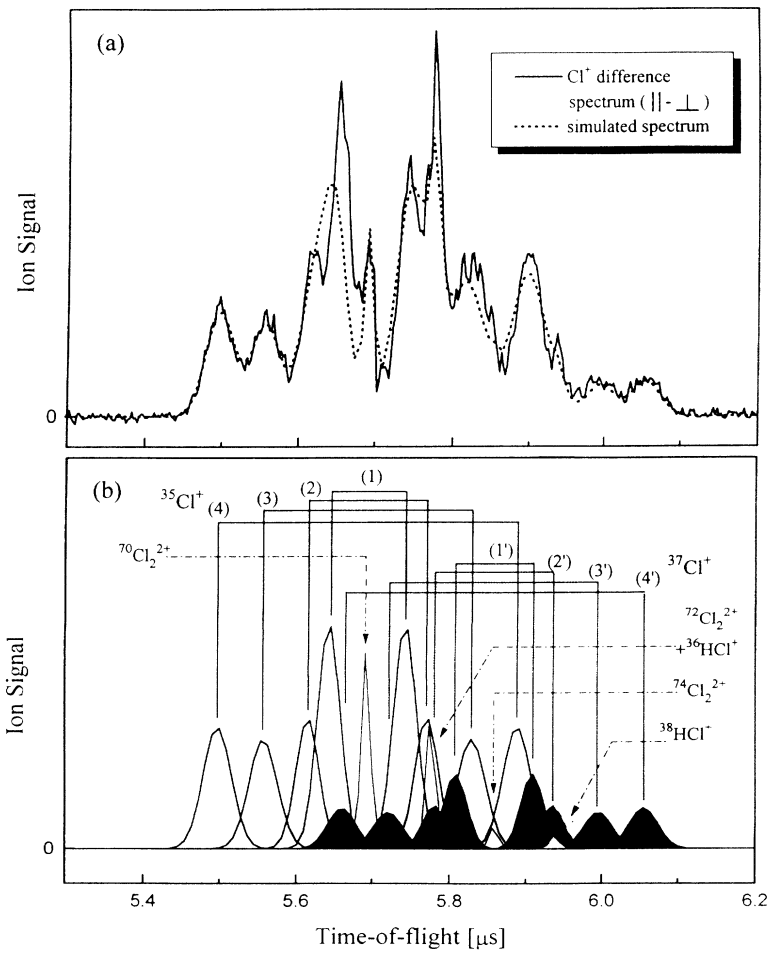

FIG. 2. Part of the TOF mass spectrum (same conditions as in Fig. 1) obtained from the MEDI of Cl_2 showing (a) the Cl difference spectrum, obtained from the subtraction of the parallel and the perpendicular spectrum [Figs. 1(a) and 1(b), respectively], and (b) the four simulated forward-backward $^{35}Cl^+$ (1,2,3,4) and $^{37}Cl^+$ (1′,2′,3′,4′) ion peaks, as well as four residual molecular ion peaks (see text).

during interaction, since its neutral ground-state vibrational period is about 60 fs. The kinetic-energy defect observed could then arise from an increase of the internuclear distance of the molecular ions, which starts to dissociate during the laser pulse. In order to check this hypothesis, the interaction dynamics should be investigated with pulses quite a bit shorter or longer than 100 fs. Since very short laser pulses in the range of 20–30 fs are not easily available at a high energy level, we have chosen to perform the MEDI of Cl_2 with 2-ps pulses at 610 nm. Although the laser pulses are not perfectly bandwidth limited, the presence of a Lyot filter in the oscillator cavity reduces the bandwidth to about 0.4 nm, which avoids any fluctuation of the laser pulse faster than 1 ps.

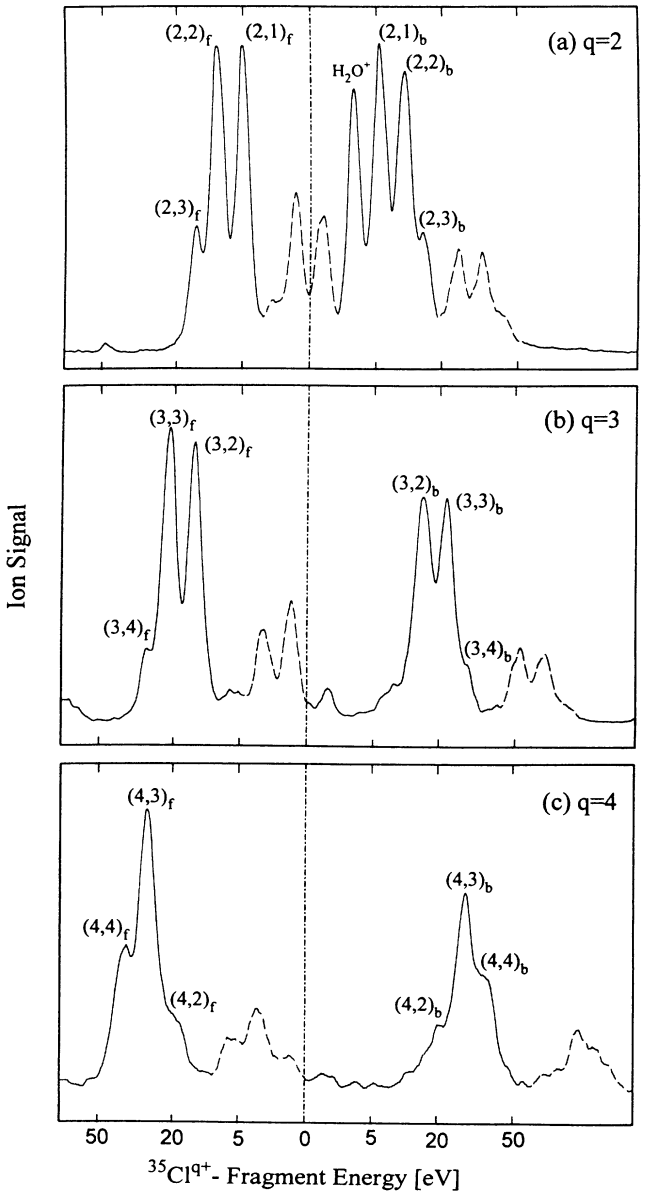

FIG. 3. Parts of the TOF mass spectrum obtained from the MEDI of Cl_2 (same conditions as in Fig. 1) showing the (a) Cl^{2+}, (b) Cl^{3+}, and (c) Cl^{4+} fragment ions on the same absolute energy scale in eV. The laser polarization is set parallel to the detection axis. The labels $(p,q)_f$ and $(p,q)_b$ indicate the respective forward and backward ion peak assigned to the (p,q) channel. The $^{37}Ce^{9+}$ ion signals are plotted in dashed line.

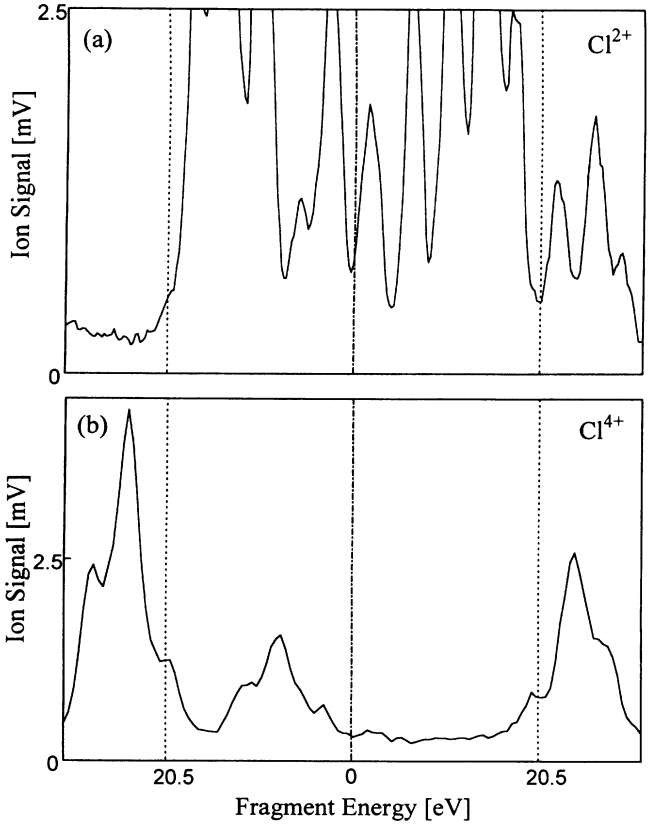

FIG. 4. Part of the TOF mass spectra of Cl_2 showing the (a) Cl^{2+} and (b) Cl^{4+} fragment ions coming from the MEDI of Cl_2 (same conditions as in Fig. 1). The two spectra are presented on the same energy scale. The Cl^{2+} signals are enlarged to focalize on those ions which are correlated to Cl^{4+} fragments with an energy of 20.5 eV i.e., the fragments of the (2,4) channel.

Figure 7 shows a comparison of the Cl_2 TOF mass spectra in the region of the Cl^{2+}, Cl^{3+}, and Cl^{4+} peaks, obtained with 130-fs pulses at 790 nm [Fig. 7(a)] and 2-ps pulses at 610 nm [Fig. 7(b)], for equal intensities $I=10^{15}$/W/cm^2. As a matter of fact, the two spectra are

TABLE I. Measured kinetic-energy releases E_{expt} from the MEDI of Cl_2 with 130-fs pulses at 790 nm, for a laser intensity of 2×10^{16} W/cm^2. Channel (p,q) refers to the fragmentation channel $Cl_2^{(p+q)+}\rightarrow Cl^{p+}+Cl^{q+}$. The Coulomb energies E_{Cb} are calculated for an internuclear distance of $R_e=2$ Å. The ratio E_{expt}/E_{Cb} is also given.

Channel (p,q)	E_{expt} (eV)	E_{Cb} (eV)	E_{expt}/E_{Cb} (%)
(1,1)	5.0±0.5	7.2	69
(1,2)	10.7±0.8	14.4	74
(2,2)	20.1±1.0	28.8	70
(2,3)	30.2±1.5	43.2	70
(2,4)	41.0±5.0	57.6	71
(3,3)	44.3±3.0	64.8	68
(3,4)	60.5±5.0	86.4	70
(4,4)	78.2±8.0	115.2	68

almost identical. As a consequence, the kinetic-energy releases and the branching ratios are clearly independent of the laser pulse duration, since the laser pulse durations in Figs. 7(a) and 7(b) differ by a factor of 15.

D. The role of postdissociation ionization (PDI)

The final point concerns the problem of whether PDI falsifies the present assignments of the fragmentation channels, thus explaining why we do not detect the Coulomb energies E_{Cb} but $0.7E_{Cb}$. Actually, if PDI occurs, it cannot change the fragment energies since the electron (being much lighter than the ion) takes away the excess photon energy. In Fig. 8, however, post-ionized fragments are not observed. Despite the abundance of 0.3 eV Cl^+ ions at 395 nm, we do not detect any Cl^{2+} or Cl^{3+} ions with the same energy. This observation implies that the $Cl_2^+ \rightarrow Cl^+ + Cl + 0.6$ eV decay path is relatively slow and must occur after extinction of the laser pulse. For all wavelengths, we observe a strong signal of Cl^{2+} fragments with an energy of 5 eV coming from the (1,2) channel, but there is no trace of Cl^{3+} ions with the same energy (see, for example, Fig. 3). This observation again suggests that the molecular dissociation occurs after extinction of the laser pulse.

A second possibility to check whether PDI occurs is to compare the energy $E_{expt}(p,q)$ released by channel (p,q) to the Coulomb energies expected for $(p-1,q)$, $(p-1,q-1)$, or of even lower channels. This comparative test, however, is only significant for the low (p,q) channels, since, for the higher channels, the absolute error bar on the value of E_{expt} becomes too important. For example, the presently measured kinetic-energy releases for the (1,2) and (2,2) channels (Table I) do not fit by far the Coulomb energies of their respective lower channels. We can conclude that PDI of the fragments does not occur in our experiment, even with 2-ps pulses. Therefore, PDI cannot be invoked to explain the origin of the

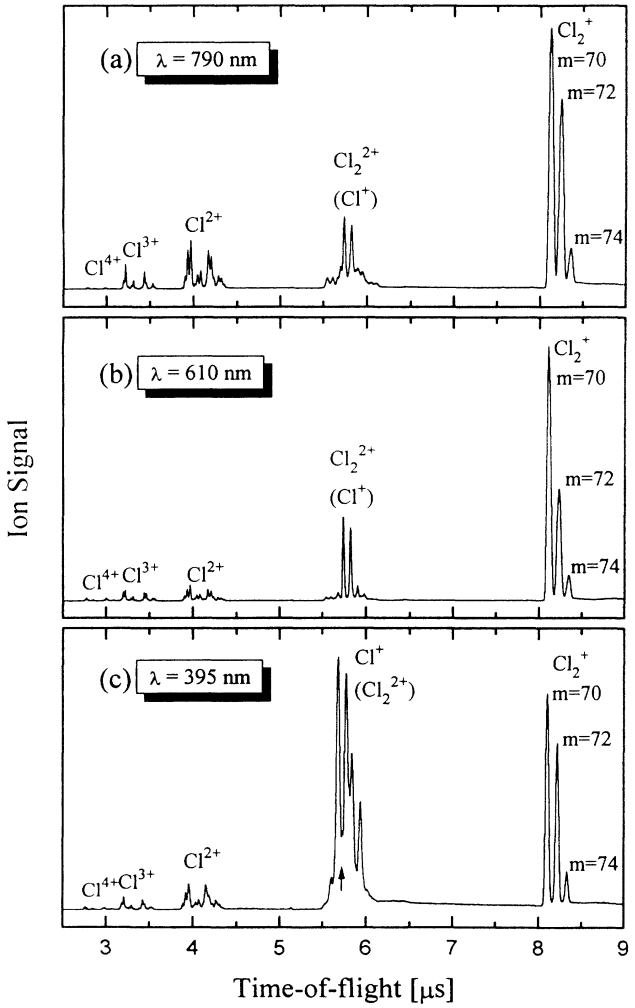

FIG. 5. TOF mass spectra of Cl_2 obtained for three different laser wavelengths: (a) 790 nm, (b) 610 nm, (c) 395 nm. The laser pulse duration is 130, 100, and 130 fs, respectively, and the laser intensity is always in the range of 10^{15} W/cm^2 (see text). The laser polarization is set parallel to the detection axis. A peak assignment is given in the figure. The arrow points at the position of the zero-energy ions with $m/q = 35$ (TOF ≈ 5.75 μs).

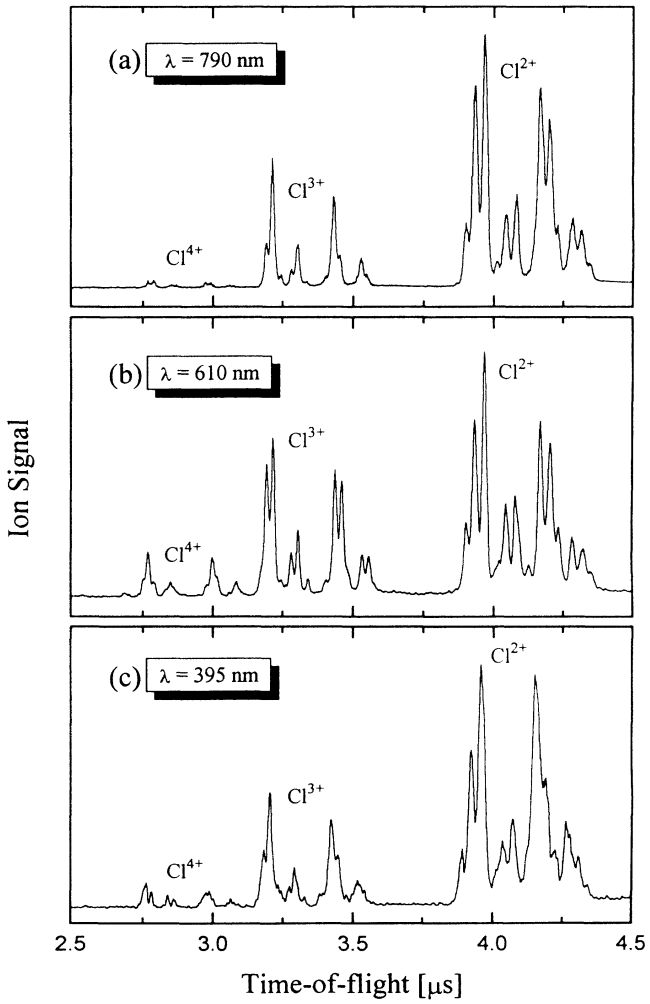

FIG. 6. Enlargement of Fig. 5, showing Cl^{2+}, Cl^{3+}, and Cl^{4+} fragment ions obtained for three different laser wavelengths: (a) 790 nm, (b) 610 nm, (c) 395 nm (same conditions as in Fig. 5).

non-Coulomb energies in the MEDI of the chlorine molecule.

IV. DISCUSSION

A. The MEDI dynamics of chlorine

In the classic picture of MEDI dynamics (cf. Introduction), the ionization of the molecule is supposed to follow a sequential scheme, in which the electrons are successively stripped off in the leading edge of the pulse. This implies for long-pulse experiments that (i) the internuclear distance successively increases due to the electrostatic repulsion force, (ii) the energy ratio $E_{\text{expt}}/E_{\text{Cb}}$ stepwise decreases with increasing charge $p+q$, and (iii) after dissociation the fragments will be post-ionized by the laser. Our observations, however, cannot be explained in the frame of this classic picture: (i) the unusual high-kinetic-energy releases, which are $\approx 70\%$ of E_{Cb} in all channels, even with pulse durations 30 times longer than the vibrational period of the molecule, and (ii) the absence of PDI with pulse durations of 2 ps.

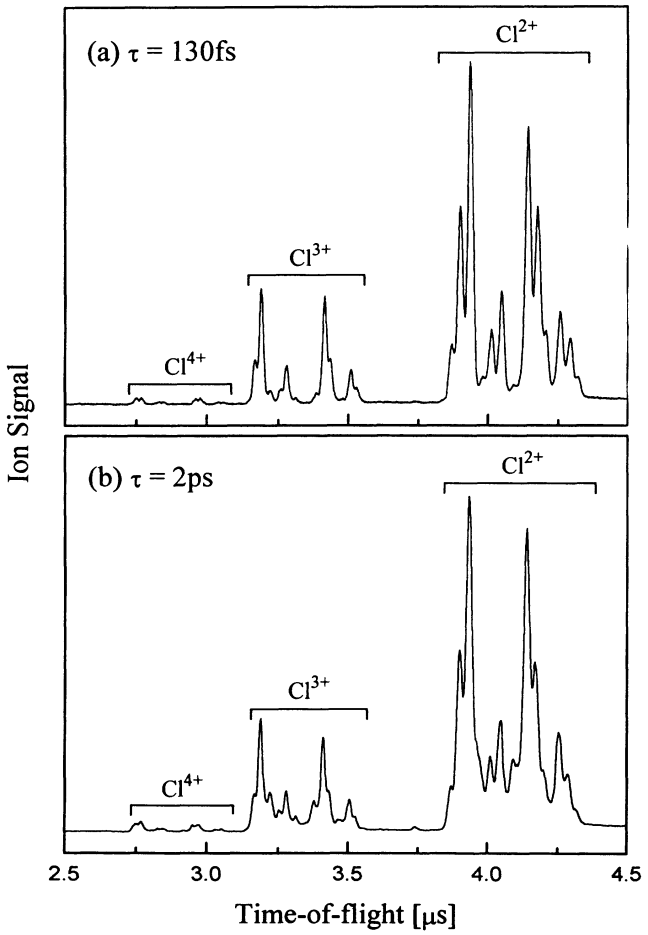

FIG. 7. Comparison of the TOF mass spectra obtained from the MEDI of Cl_2 with (a) 130-fs pulses at 790 nm, and (b) 2-ps pulses at 610 nm with the same laser intensities of 10^{15} W/cm^2. In both spectra the laser polarization is set parallel to the detection axis.

Therefore, we are led to speculate that the molecular dissociation occurs at the end of the laser pulse. This is only possible if the molecule is somehow *trapped* by the laser field via the electronic interactions which compensate for the internuclear electrostatic repulsion. Codling and Frasinsky [2] have recently pointed out that even a single electron, constrained to lie midway between two positive ions, can overcome the repulsion of a seven-times-ionized molecule. In the model we propose, the valence electrons, which are strongly coupled to the laser field, are not ejected but remain bound in light-induced states of the molecule. Recently, Bandrauk, Aubanel, and Gauthier [15] and Dietrich *et al.* [16] have postulat-

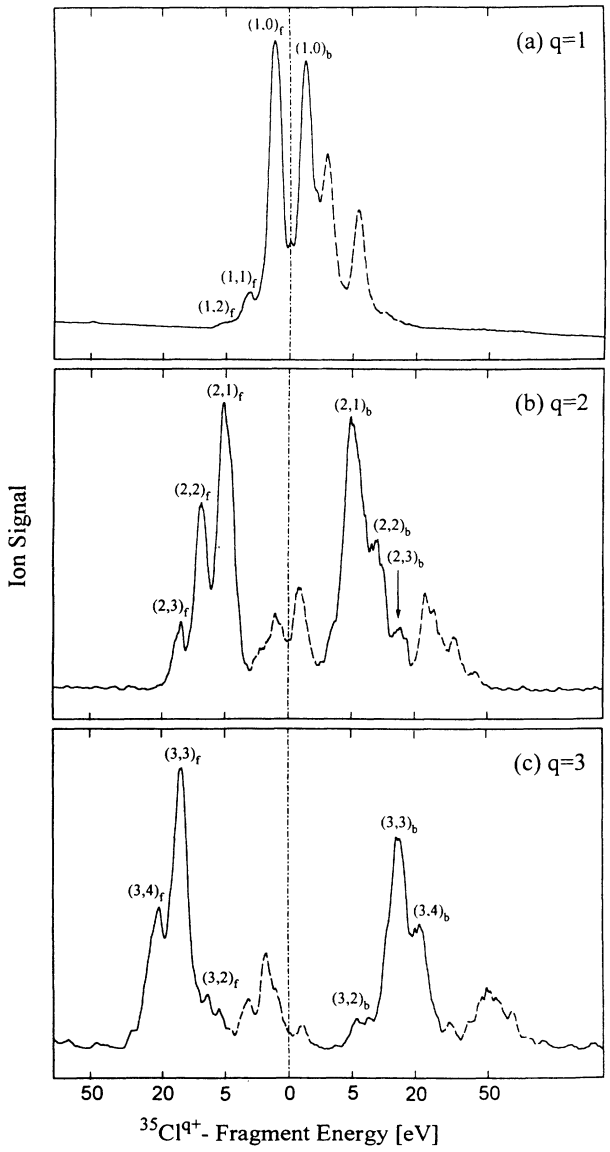

FIG. 8. Parts of the TOF mass spectrum obtained from the MEDI of Cl_2 with 130-fs pulses at 395 nm ($I=2\times10^{15}$ W/cm^2) showing the (a) Cl^+, (b) Cl^{2+}, and (c) Cl^{3+} fragment ions on the same absolute energy scale in eV. The laser polarization is set parallel to the detection axis. The labels $(p,q)_f$ and $(p,q)_b$ indicate the respective forward and backward ion peak assigned to the (p,q) channel.

ed that such field-induced nonlinear effects in molecules arise from transitions between charge-transfer or charge-resonance states (for even or odd charged molecules, respectively), which were first introduced by Mulliken [17]. The authors point out that the transition moments between these states are very large and therefore dominate nonresonant interactions in intense laser fields. The coupling of these molecular states involves electronic motion at the internuclear scale. From the observation that the ion fragments are ejected along the laser electric field, we believe that the large dipole moments of such laser-trapped molecules are also at the origin of the laser-induced molecular alignment. The electrons should then oscillate along the axis of the laser-trapped molecular species, that is, along the laser electric field.

The concept of light-induced bound states was first introduced by Fedorov *et al.* [18], Yuan and George [19], and Bandrauk and Sink [20] in the framework of time-independent calculations at specific intensities. Recently, population trapping in molecular dressed states has been predicted [21,22] and observed [23] in the case of H_2^+, where the radiative coupling between the ground state ($1s\sigma_g$) and the first repulsive state ($2p\sigma_u$) induces a new adiabatic potential well for laser intensities around 10^{14} W/cm^2. In these cases, trapping is only achieved in a small intensity range. If the intensity is too low, the adiabatic curve will not support the trapped population. If the intensity is too strong, the trapped population will escape. In contrast, the trapping mechanism observed for chlorine appears quite robust against the laser intensity. Moreover, trapping of the population is very efficient, even on the picosecond time scale, since no post-ionized fragments have been observed.

B. Comparison with the MEDI processes of other molecules

The MEDI picture we propose for Cl_2 appears also to be consistent with the results obtained for other molecules: (i) the molecular stabilization also holds for the diatomics such as H_2 [24,26], CO, O_2, and N_2 [7], and for bigger molecules like CO_2 [25] and C_2H_2 [8], since, for these systems, the energy ratio $E_{\text{expt}}E_{\text{Cb}}$ has been found to be almost constant for all fragmentation channels; (ii) the energy releases have been shown to be robust against the laser pulse duration.

Table II recapitulates the energy ratio $E_{\text{expt}}/E_{\text{Cb}}$ as well as the internuclear distance R_e for all these molecules (R_e is used to calculate E_{Cb}). The diatomics with an equilibrium internuclear distance close to 1.1 Å release about 45% of the Coulomb energies. The CO_2, C_2H_2, or C_2H_4 molecules for which the C—O or C—C bond distances are close to 1.2 Å release about 50% of the Coulomb energies [8,25]. For Cl_2 ($R_e=2.0$ Å) we find $E_{\text{expt}}/E_{\text{Cb}}=70\%$, and experiments on iodine [3] ($R_e=2.67$ Å) indicate a slightly higher energy ratio of 75%.

The compilation in Table II shows the tendency that (i) the agreement of the experimental kinetic-energy releases with the predictions of the point-charge model improves for more elongated molecules and (ii) the molecular mass does not appear to have a strong influence on the Coulomb explosion dynamics, since H_2 ($m=2$) and N_2 ($m=28$) behave similarly, as do Cl_2 ($m=70$) and I_2 ($m=254$).

TABLE II. Compilation of the experimentally deduced energy ratios $E_{\text{expt}}/E_{\text{Cb}}$ (%), representing the mean value of all fragmentation channels, from MEDI of different molecules. The internuclear separation R_e (Å), which yields the F_{Cb} value, is taken as that of the neutral ground-state molecule (or that of the singly charged molecular ion when the two distances are different). This choice is valid, since all MEDI experiments have concluded that the first step of the interaction is the formation of the singly charged molecular ion. The coefficient a, relating R_e and the effective internuclear distance R_{eff} at which Coulomb explosion is believed to occur (see text), is also given.

Molecule	R_e (Å)	$E_{\text{expt}}/E_{\text{Cb}}$ (%)	$a=\sqrt{R_e}/(E_{\text{expt}}/E_{\text{Cb}})$	Ref.
H_2	1.1	40[a]	2.6[a]	[26]
CO	1.1	43	2.4	[7]
N_2	1.1	47	2.2	[7]
O_2	1.1	42	2.5	[7]
C_2H_2	1.2[b]	50[b]	2.2[b]	[8]
CO_2	1.2	50	2.2	[25]
Cl_2	2.0	70	2.0	This work
I_2	2.7	75	2.2	[3]

[a]Values obtained for the H^+ peak with an energy of 2.65 eV.
[b]The indicated value concerns the C—C bond.

It is interesting to note that the experimental energies, obtained for the molecules in Table II, all seem to result from a Coulomb explosion occurring at the effective internuclear distance $R_{\text{eff}}=a\sqrt{R_e}$. The proportionality factor a, given in Table II, is found to be independent of the molecule ($a\approx 2.3$). In conclusion, it turns out that the kinetic-energy releases observed do not significantly depend on the experimental conditions, such as laser pulse duration, wavelength, or intensity, but are mainly determined by the molecule itself, i.e., the effective internuclear distance at which stabilization occurs.

V. CONCLUSION

We have investigated the MEDI of Cl_2 under various experimental conditions and come to the following conclusions: (1) The kinetic-energy releases are about 70% of the Coulomb energies and do not significantly depend on the experimental conditions, such as laser pulse duration (100 fs $\leq\Delta\tau\leq$ 2 ps), wavelength ($395\leq\lambda\leq 790$ nm), or intensity ($10^{15}\leq I\leq 2\times 10^{16}$ W/cm^2). This result stands for all observed fragmentation channels up to $Cl_2^{8-}\rightarrow Cl^{4+}+Cl^{4+}$, which demonstrates that Coulomb repulsion is actually the prevailing process governing the MEDI interaction. (2) The postdissociation ionization of the fragments is not observed even with 2-ps pulses. (3) There is a clear tendency for MEDI of quite elongated molecules, such as Cl_2 or I_2, to result in kinetic-energy releases approaching the Coulomb energies. (4) All the main (p,q) fragmentation channels observed are charge-symmetric ($|p-q|<2$). The only asymmetric channel observed is the (2,4) channel of Cl_2^{6+}, which is about 15 times weaker than the corresponding (3,3) channel.

Finally, we speculate that an efficient field-induced stabilization of chlorine occurs, where the molecule is *trapped* by the laser field via the electronic interaction, which compensates for the internuclear electrostatic repulsion. According to recent theoretical work, we believe that this population trapping is due to strong charge-transfer or charge-resonance coupling in the presence of the intense laser field. Therefore, it appears that kinetic-energy releases do not depend on the experimental conditions, but are mainly determined by the molecule itself, i.e., the effective internuclear distance at which stabilization occurs. This hypothesis of laser-induced trapping calls for further experimental and theoretical confirmations.

ACKNOWLEDGMENTS

The authors are grateful to Professor A. Giusti-Suzor and Dr. P. Corkum for fruitful discussions, to P. D'Oliveira and P. Meynadier for expertly operating the Ti:Sa laser system, and to M. Bougeard and E. Caprin for their skilled technical assistance.

[1] D. Normand and C. Cornaggia, Laser Phys. **3**, 664 (1993), and references therein.
[2] K. Codling and L. J. Fransinsky, J. Phys. B **26**, 783 (1993).
[3] M. Schmidt, D. Normand, and C. Cornaggia (unpublished results). The results of Dietrich, Strickland, and Corkum (Ref. [6] of the present manuscript) do not contain explicit values on the experimental kinetic-energy releases, but appear consistent with our data.
[4] M. Brewczyk and L. J. Fransinski, J. Phys. B **24**, L307 (1991).
[5] C. Cornaggia, J. Lavancier, D. Normand, J. Morellec, and H. X. Liu, Phys. Rev. A **42**, 5464 (1990).
[6] P. Dietrich, D. T. Strickland, and P. B. Corkum, J. Phys. B **26**, L1 (1993).
[7] C. Cornaggia, J. Lavancier, D. Normand, J. Morellec, P. Agostini, J. P. Chambaret, and A. Antonetti, Phys. Rev. A **44**, 4499 (1991).
[8] C. Cornaggia, D. Normand, and J. Morellec, J. Phys. B **25**, L415 (1992).
[9] Z. Bor, J. Mod. Opt. **35**, 1907 (1988).
[10] P. A. Hatherly, L. J. Hatherly, K. Codling, A. J. Langley, and W. Shaikh, J. Phys. B **23**, L291 (1990).
[11] D. Normand, L. A. Lompré, and C. Cornaggia, J. Phys. B **25**, L497 (1992).
[12] L. J. Fransinski, K. Codling, and P. A. Hatherly, Science **246**, 1029 (1989).
[13] J. H. Beynon, R. M. Caprioli, and J. W. Richardson, J. Am. Chem. Soc. **21**, 1852 (1971).
[14] P. G. Fournier, J. Fournier, F. Salama, D. Stärk, S. D. Peyerimhoff, and J. H. D. Eland, Phys. Rev. A **34**, 1657 (1986).
[15] A. D. Bandrauk, E. E. Aubanel, and J.-M. Gauthier, in *Molecules in Laser Fields,* edited by A. D. Bandrauk (Dekker, New York, 1994), p. 109.
[16] P. Dietrich, P. B. Corkum, D. T. Strickland, and M. Laberge, in *Molecules in Laser Fields* (Ref.[15]), p. 181.
[17] R. S. Mulliken, J. Chem. Phys. **7**, 20 (1939).
[18] M. V. Fedorov, O. V. Kudrevatova, V. P. Makarov, and A. A. Samokhin, Opt. Commun. **13**, 299 (1975).
[19] M. Yuan and T. S. George, J. Chem. Phys. **68**, 3040 (1978).
[20] A. D. Bandrauk and M. L. Sink, J. Chem. Phys. **74**, 1110 (1981).
[21] A. Giusti-Suzor and F. H. Mies, Phys. Rev. Lett. **68**, 3869 (1992).
[22] F. H. Mies, A. Giusti-Suzor, E. Charron, L. F. DiMauro, and B. Yang (unpublished).
[23] A. Zavriyev, P. H. Bucksbaum, J. Squier, and F. Saline, Phys. Rev. Lett. **70**, 1077 (1993).
[24] L. J. Frasinski, M. Stankiewicz, P. A. Hatherly, G. M. Cross, K. Codling, A. J. Langley, and W. Shaikh, Phys. Rev. A **16**, R6789 (1992).
[25] C. Cornaggia, M. Schmidt, and D. Normand, J. Phys. B **27**, L123 (1994).
[26] M. Schmidt, D. Normand, and C. Cornaggia (unpublished results).